


 Cite this: *RSC Adv.*, 2020, **10**, 6022

Zinc(II)-based coordination polymer encapsulated Tb³⁺ as a multi-responsive luminescent sensor for Ru³⁺, Fe³⁺, CrO₄²⁻, Cr₂O₇²⁻ and MnO₄⁻†

 Yuandi Wu,^a Dongyang Liu,^a Meihua Lin^a and Jing Qian *^{abc}

A zinc(II)-based coordination polymer (CP), namely [Zn(modbc)₂]_n (Zn-CP) (modbc = 2-methyl-6-oxygen-1,6-dihydro-3,4'-bipyridine-5-carbonitrile), has been synthesized and characterized. Single-crystal structural determination reveals that Zn-CP is a two-dimensional framework structure with tetranuclear homometallic Zn₄(modbc)₄ units cross-linked by modbc. The excellent luminescence as well as good stability of Zn-CP do not enable it to have selective sensing capability for different ions. After encapsulation of Tb³⁺ in Zn-CP, the as-obtained fluorescent functionalized Tb³⁺@Zn-CP maintained excellent luminescence as well as stability, which made it a highly selective and sensitive multiresponsive luminescent sensor for Ru³⁺, Fe³⁺, CrO₄²⁻, Cr₂O₇²⁻, and MnO₄⁻ with high sensitivity, good anti-interference performance, and quick response time (~10 s). The detection limits are 0.27 μM, 0.57 μM, 0.10 μM, 0.43 μM and 0.15 μM, respectively. A possible sensing mechanism was discussed in detail.

 Received 15th November 2019
 Accepted 28th January 2020

DOI: 10.1039/c9ra09541a

rsc.li/rsc-advances

1. Introduction

At present, hexavalent chromium (CrO₄²⁻, Cr₂O₇²⁻) as a potential carcinogen mainly exists in natural water and various industrial processes, which can cause serious harm to the environment and human health.^{1,2} In addition, the extensive application of MnO₄⁻ in research experiments and industry has caused serious water pollution.³ On the other hand, Fe³⁺ affects the activity of hemoglobin and transferrin in organisms. Both excess and deficiency of the normal permissible limit will lead to serious diseases.^{4,5} The purification and trace detection of ruthenium have been paid attention to,⁶ and the olefin reaction catalyzed by ruthenium also won the 2005 Nobel Prize in chemistry.⁷ The development of ion selective sensing is very important in life and environmental science, so new materials for detecting Ru³⁺, Fe³⁺, CrO₄²⁻, Cr₂O₇²⁻, and MnO₄⁻ have attracted great attention.⁸⁻¹¹ To date, various methods and techniques for ion detection have been reported.¹²⁻¹⁴ Among them, fluorescent chemosensors have attracted extensive research interest due to their remarkable advantages such as fast response, high sensitivity and simplicity.¹⁵⁻¹⁷

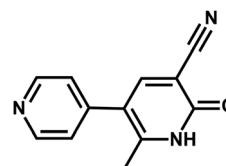
3D microporous CPs can produce significant fluorescence signals and visible emission, and has become the most reported chemosensors.¹⁸⁻²² At present, Ln-CPs, compared with transition metal-based CPs, has attracted great interest due to its unique optical characteristics, such as large Stokes shift and long fluorescence lifetime obtained by “antenna effect” of 4f–4f electron transition.^{19,20,23,24} Recently, lanthanide ions were doped into CPs by post-synthesis method (PSM), and an alternative strategy to construct Ln-CPs and optimize photoluminescence was proposed.^{25,26} Any desired fluorescent probe can be obtained by changing the molar ratio of reactants.^{27,28}

Some luminescent CPs have been developed in recent years to effectively simultaneously sense Fe³⁺ and Cr₂O₇²⁻.^{29,30} The reported polymer as a fluorescent probe for the specific detection of MnO₄⁻ contaminants is still rare to date.^{31,32} However, there is no multifunctional ion sensor for sensing Ru³⁺, Fe³⁺, CrO₄²⁻, Cr₂O₇²⁻ and MnO₄⁻ at the same time. Moreover, low-dimensional chemosensors with one-dimensional or two-dimensional structures are rarely reported as ion sensors.³³ Herein, asymmetric unflexible 2-methyl-6-oxygen-1,6-dihydro-3,4'-bipyridine-5-carbonitrile (modbc) containing coordination N and O atoms, was utilized as an anionic ligand

^aCollege of Chemistry, Tianjin Normal University, Tianjin 300387, P. R. China. E-mail: qianjing@aliyun.com
^bTianjin Key Laboratory of Structure and Performance for Functional Molecules, Tianjin Normal University, Tianjin 300387, P. R. China

^cKey Laboratory of Inorganic–Organic Hybrid Functional Materials Chemistry, Tianjin Normal University, Ministry of Education, Tianjin 300387, P. R. China

† Electronic supplementary information (ESI) available: Crystallographic data, tables, IR, UV, TGA, PXRD, ICP, XPS, and luminescent spectra. CCDC 1882227. For ESI and crystallographic data in CIF or other electronic format see DOI: 10.1039/c9ra09541a



Scheme 1 The structure of modbc.



(Scheme 1). A new compound with the formula, $[\text{Zn}(\text{modbc})_2]_n$ (Zn-CP) has been obtained *via* solvothermal reaction showing a new type of two-dimensional open framework structure. To improve the selectivity of Zn-CP, $\text{Tb}^{3+}@\text{Zn-CP}$ was obtained *via* PSM. $\text{Tb}^{3+}@\text{Zn-CP}$ detect a series of metal ions and anions by taking the advantage of its excellent luminescence and good stability. The results demonstrate that $\text{Tb}^{3+}@\text{Zn-CP}$ is an efficient multiresponsive sensor for optical detection of Ru^{3+} , Fe^{3+} , CrO_4^{2-} , $\text{Cr}_2\text{O}_7^{2-}$ and MnO_4^- with a fast response of 10 s and lower limit of detection.

2. Experimental section

2.1 General methods and materials

Materials. Chloride or nitrate salt of Ag^+ , Pb^{2+} , Mn^{2+} , Hg^{2+} , Ni^{2+} , Ca^{2+} , Cd^{2+} , Zn^{2+} , Co^{2+} , Cu^{2+} , Fe^{3+} , Ru^{3+} were purchased from Sigma-Aldrich and used as received. Potassium salt of I^- , $\text{C}_2\text{O}_4^{2-}$, CrO_4^{2-} , $\text{Cr}_2\text{O}_7^{2-}$, SO_4^{2-} , CO_3^{2-} , HCO_3^- , PO_4^{3-} , MnO_4^- and $(\text{NH}_4)_2\text{Fe}(\text{SO}_4)_2$ were analytical grade and used without purification. Water purified in a Milli-Q water filtration system to a resistance of $18 \text{ m}\Omega \text{ cm}^{-1}$, was used in all measurement experiments. Diethylether and dimethyl formamide (DMF) were purified by standard methods.

Apparatus. Element analysis (C, H and N), electronic and infrared spectra were measured with PerkinElmer analyzer model 240 spectrometer, JASCO V-570 spectrometer and Bruker Vector 22 FT-IR spectrometer, respectively. Thermogravimetric analysis (TGA) was performed by a heating rate of 10 K min^{-1} with Netzsch STA409PC Thermal Analyzer. Powder X-ray diffraction (PXRD) was investigated by Bruker D8 diffractometer at 40 KV, 40 mA, copper target tube and graphite monochromator. The X-ray diffraction data were collected with a Bruker APEX-II CCD diffractometer with graphite monochromated $\text{Mo-K}\alpha$ radiation ($\lambda = 0.71073 \text{ \AA}$) at 296 K. The structure was solved by the standard crystallographic program SHELXS-97 and SHELXL-97 and refined with full-matrix least-squares on F^2 .^{34,35} The emission spectra were detected by Spex Fluorog-2 spectrofluorimeter (model F111, Spex Industries, Edison, NJ, USA). The spectrometer uses 450 W xenon lamp (XBO 450 W/1, Osram, Germany) as excitation light source and 950 V photomultiplier tube (R928, Hamamatsu, Japan) as detector.

2.2 Synthesis of $[\text{Zn}(\text{modbc})_2]_n$ (Zn-CP)

A mixture of ZnSO_4 (0.05 mmol, 0.008 g) and modbc (0.1 mmol, 0.021 g) was dissolved in 8 mL of DMF/ H_2O (1 : 3), and stirred at room temperature for 15 min. Then the mixture was transferred into a 25 mL Teflon-lined stainless steel vessel. The reactor was heated to $120 \text{ }^\circ\text{C}$ for 72 h under self-generated pressure, then cooled to ambient temperature at a rate of $2.0 \text{ }^\circ\text{C h}^{-1}$. Finally, light yellow bulk-shaped crystals were collected, filtered, washed with H_2O ($3 \times 1 \text{ mL}$), diethylether ($3 \times 1 \text{ mL}$). The total yields of is *ca.* 68% based on the metal ions. Elem. anal. calcd for $\text{C}_{12}\text{H}_8\text{Zn}_{0.50}\text{N}_3\text{O}$: C, 59.33; H, 3.32; N, 17.30%. Found: C, 58.63; H, 4.02; N, 16.87%. IR (KBr pellet, cm^{-1}): $\nu = 3370.13$ (vs),

2984.28 (s), 2340.06 (m), 1602.97 (s), 1385.90 (s), 1108.44 (vs), 982.48 (vs), 857.44 (s), 538.28 (vs) (Fig. S1†).

2.3 Preparation of $\text{Tb}^{3+}@\text{Zn-CP}$

$\text{Tb}^{3+}@\text{Zn-CP}$ was prepared by soaking 200 mg powder of Zn-CP in 1.0 mM $\text{Tb}(\text{NO}_3)_3$ aqueous solution for 24 h, centrifuged, washed with Milli-Q water to remove the remaining Tb^{3+} , and dried under $60 \text{ }^\circ\text{C}$ vacuum conditions for tonight.

2.4 General fluorescence measurements

Zn-CP and $\text{Tb}^{3+}@\text{Zn-CP}$ (100 μM) were well-dispersed in DMF by sonicating for 30 min to obtain stock solution and stored in a $4 \text{ }^\circ\text{C}$ refrigerator. The aqueous solution of nitrate salt or chloride of Ag^+ , Pb^{2+} , Mn^{2+} , Hg^{2+} , Ni^{2+} , Ca^{2+} , Cd^{2+} , Zn^{2+} , Co^{2+} , Cu^{2+} , Fe^{3+} , Ru^{3+} (1.0 mM) were prepared for luminescent experiments. Generally, ferrous salt is easy to be oxidized in the air, but it is relatively stable and not easy to be oxidized after forming double salt, so we chose double salt $(\text{NH}_4)_2\text{Fe}(\text{SO}_4)_2$ to prepare the aqueous solution of Fe^{2+} . In addition, the same concentrations (1.0 mM) of aqueous solution containing potassium salt of I^- , $\text{C}_2\text{O}_4^{2-}$, CrO_4^{2-} , $\text{Cr}_2\text{O}_7^{2-}$, SO_4^{2-} , CO_3^{2-} , HCO_3^- , PO_4^{3-} , MnO_4^- were also prepared.

Fluorescence emission spectra of Zn-CP and $\text{Tb}^{3+}@\text{Zn-CP}$ in 1 cm path length quartz cuvette were measured by a Spex Fluorog-2 spectrofluorimeter. 1.0 mM above ions were added to a quartz cuvette for luminescence detection immediately by excitation with 330 nm. The slit size for both excitation and emission was 4 nm. The fluorescence stability of Zn-CP and $\text{Tb}^{3+}@\text{Zn-CP}$ with different pH values were investigated in 5 mM Tris-HCl/NaCl buffer. The Stern-Volmer equation: $I_0/I = 1 + K_{sv}[Q]$ was applied to judge the quenching effect.³⁶ The detection limit was calculated according to $3\sigma/k$ recommended by IUPAC, where the standard deviation, σ value was estimated by 15 repeated fluorescent measurements of Zn-CP and $\text{Tb}^{3+}@\text{Zn-CP}$, and k value was obtained using a calibration curve of I vs. $[Q]$.³⁷

3. Results and discussion

3.1 Description of structure

A 2D CP was synthesized by self-assemble of ZnSO_4 and modbc by one-pot solvothermal method with a yield of $\sim 68\%$. X-ray crystallographic analysis shows that Zn-CP crystallizes in the tetragonal space group $P4_32_12$, $Z = 28$ (Table S1†). The symmetric unit consists of one Zn^{2+} center and two modbc anions. In Zn-CP, each Zn(II) center has a distorted octahedral geometry and it is connected to two O atoms from two modbc ligands and four N atoms from four modbc ligands, as shown in Fig. 1a. Fig. 1b displays that each modbc molecule adopts tridentate coordination mode. The Zn-O distance is 2.390 Å , while the Zn-N length is in the range of 2.089–2.104 Å . The L-Zn-L (L = O, N) bond angle is in the scope of $59.10(8)$ – $173.81(11)^\circ$ (Table S2†). In addition, the structure of Zn-CP is characterized in that each zinc chain serves as a secondary construction unit and is further connected into a 2D framework through modbc ligands, and the framework comprises the tetranuclear homometallic



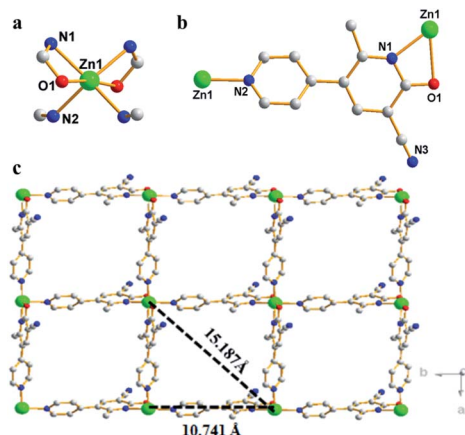


Fig. 1 (a) Coordination environment of Zn^{2+} in Zn-CP. (b) Coordination mode of modbc molecule. (c) Two-dimensional reticulated structure of Zn-CP along the c axis; red, O; gray, C; green, Zn1; blue, N. All H atoms are omitted for clarity.

$\text{Zn}_4(\text{modbc})_4$ units with different $\text{Zn1}\cdots\text{Zn1}$ distances of 10.741 and 15.187 Å (Fig. 1c), which is larger than $\text{Cd1}\cdots\text{Cd1}$ distances of 10.434 and 14.756 Å.³⁸

3.2 Property characterization

TGA analysis of Zn-CP was measured to evaluate its thermal stability at ≤ 500 °C, as shown in Fig. S2.† PXRD confirmed that Zn-CP has phase purity and excellent stability in H_2O , common organic solvents and metal salt aqueous system (Fig. S3.†). In addition, the corresponding PXRD after the sample was heated at different temperatures for 8 h showed that Zn-CP skeleton still had excellent chemical stability at ≤ 180 °C, as shown in Fig. S4.† High stability of Zn-CP may be due to the synergy between N/O atoms and Zn^{2+} according to Pearson's hard/soft acid-base principle,^{39,40} or relatively high density 2D framework, and the synergy effect of these factors.⁴¹ Obviously, the Zn-CP framework with excellent chemical stability provides the possibility for its practical application as an ion sensor.

Then, Zn-CP was soaked in $\text{Tb}(\text{NO}_3)_3$ aqueous solution to obtain $\text{Tb}^{3+}@\text{Zn-CP}$. The crystal integrity of Zn-CP remained unchanged after doping Tb^{3+} , which was confirmed by PXRD (Fig. S5.†). PXRD of $\text{Tb}^{3+}@\text{Zn-CP}$ after soaking in FeCl_3 , RuCl_3 , KMnO_4 , K_2CrO_4 and $\text{K}_2\text{Cr}_2\text{O}_7$ solutions for 12 h, respectively, also shows that it has excellent crystal integrity and chemical stability. In order to obtain the amount of Tb^{3+} doped in Zn-CP, ICP analysis on $\text{Tb}^{3+}@\text{Zn-CP}$ was performed (Table S3.†). The result shows that the ratio of Zn^{2+} and Tb^{3+} is approximately 80 : 1. $\text{Tb}^{3+}@\text{Zn-CP}$ and Zn-CP were further analyzed by X-ray photoelectron spectroscopy (XPS), as shown in Fig. S6.† After being treated with Tb^{3+} , three new peaks corresponding to $\text{Tb } 3d_{3/2}$, $\text{Tb } 3d_{5/2}$, $\text{Tb } 4d$ appeared at 1277.5, 1243.0 and 153.0 eV, thus the existence of Tb^{3+} in the composite material can be determined.⁴²

3.3 Fluorescence properties

Considering that Zn-CP composed of d^{10} ions and aromatic ligand may be a promising luminescent material,⁴³ the

fluorescence properties of Zn-CP were investigated in 5 mM Tris-HCl/NaCl buffer (pH 7.0) at room temperature. Under 312 and 330 nm excitation, the luminescence of Zn-CP and $\text{Tb}^{3+}@\text{Zn-CP}$ in aqueous solution show the intense emission centered at 395 and 390 nm, respectively, while the luminescence of modbc exhibits a similar emission centered at 475 nm at 415 nm excitation. The fluorescence emission of Zn-CP and $\text{Tb}^{3+}@\text{Zn-CP}$ also show good stability within 12 h (Fig. S7.†). In addition, the fluorescence stability of Zn-CP and $\text{Tb}^{3+}@\text{Zn-CP}$ dispersed in different pH 1.0–13.0 solution were performed, as shown in Fig. S8.† Obviously, $\text{Tb}^{3+}@\text{Zn-CP}$ framework with excellent chemical stability than Zn-CP offers the possibility for its practical application based on the fact that industrial effluent and polluted rivers are usually acidic or alkaline.⁴⁴

3.4 Detection of ions

To detect water pollution, we explored the potential detection of Zn-CP to various ions. 1 mM aqueous solution of Ag^+ , Pb^{2+} , Mn^{2+} , Hg^{2+} , Ni^{2+} , Ca^{2+} , Cd^{2+} , Zn^{2+} , Co^{2+} , Cu^{2+} , Fe^{3+} , Fe^{2+} , Ru^{3+} , I^- , $\text{C}_2\text{O}_4^{2-}$, CrO_4^{2-} , $\text{Cr}_2\text{O}_7^{2-}$, SO_4^{2-} , CO_3^{2-} , HCO_3^- , PO_4^{3-} and MnO_4^- were prepared, and we investigated their effects on the fluorescence intensity of Zn-CP. All experimental cations have a remarkable effect on the luminescence intensity of Zn-CP (Fig. S9.†), and all experimental anions show negligible effect on the luminescence intensity of Zn-CP (Fig. S10.†) indicating that Zn-CP shows no selective sensing ability toward different both cations and anions.

To improve the selectivity of Zn-CP, $\text{Tb}^{3+}@\text{Zn-CP}$ was obtained *via* PSM. A series of luminescence experiments were carried out by the addition of different metal ions to $\text{Tb}^{3+}@\text{Zn-CP}$. Other metal ions have a negligible effect on the luminescence intensity of $\text{Tb}^{3+}@\text{Zn-CP}$ except Ru^{3+} and Fe^{3+} , indicating that $\text{Tb}^{3+}@\text{Zn-CP}$ can detect Ru^{3+} and Fe^{3+} selectively among coexisting ions (Fig. 2). Furthermore, the titration of $\text{Tb}^{3+}@\text{Zn-CP}$ (10 μM) with Ru^{3+} or Fe^{3+} (0.0–90 μM) were performed, as shown in Fig. S11 and S12.† With the gradual addition of Ru^{3+} or Fe^{3+} , the fluorescence of $\text{Tb}^{3+}@\text{Zn-CP}$ solution was obviously quenched.

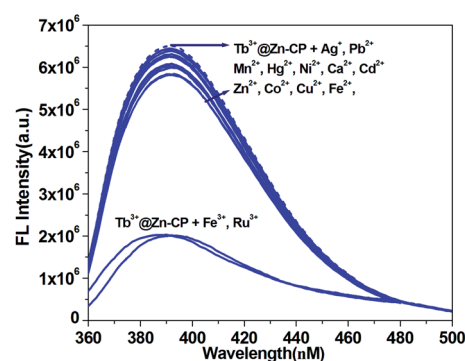


Fig. 2 Luminescence intensity of $\text{Tb}^{3+}@\text{Zn-CP}$ upon different ions (Ru^{3+} , Ag^+ , Cd^{2+} , Zn^{2+} , Pb^{2+} , Ca^{2+} , Mn^{2+} , Cu^{2+} , Co^{2+} , Ni^{2+} , Fe^{2+} , Hg^{2+} and Fe^{3+}) in 5 mM Tris-HCl/NaCl buffer (pH 7.0). [$\text{Tb}^{3+}@\text{Zn-CP}$] = 10 μM and [cations] = 50 μM . λ_{ex} : 330 nm, λ_{f} : 390 nm, slit width: 4 nm.



Compared with Ru^{3+} , the influence of Fe^{3+} on the luminescence intensity of $\text{Tb}^{3+}@Zn\text{-CP}$ is relatively smaller (Fig. 3a and b). To better analyze, the quenching sensitivity was quantified by the Stern–Volmer equation: $I_0/I = 1 + K_{sv}[Q]$.⁴⁵ At low concentrations (0–20 μM), a good linearity plot was obtained with correlation coefficient of 0.997 for Fe^{3+} and 0.994 for Ru^{3+} , respectively. Also, the quenching constant (K_{sv}) were determined to be $7.2 \pm 0.56 \times 10^3 \text{ M}^{-1}$ for Fe^{3+} and $1.72 \pm 0.19 \times 10^4 \text{ M}^{-1}$ for Ru^{3+} , respectively. However, the Stern–Volmer plot deviated from the straight line at higher concentrations due to self-absorption or energy transfer processes.^{46,47} In addition, the LODs based on $\text{Tb}^{3+}@Zn\text{-CP}$ were also obtained to be $0.57 \pm 0.06 \mu\text{M}$ for Fe^{3+} and $0.27 \pm 0.01 \mu\text{M}$ for Ru^{3+} , respectively (Fig. S13†). The calculated LOD value is far below MCL for Fe^{3+} in drinking water as required by U.S. EPA standard (5.36 μM).⁴⁸ The performance of $\text{Tb}^{3+}@Zn\text{-CP}$ composite for sensing Ru^{3+} and Fe^{3+} is comparable with some recently reported MOF composites (Table S4†).

To corroborate the practical applicability of $\text{Tb}^{3+}@Zn\text{-CP}$ as a sensor for Fe^{3+} , we performed a series of anti-jamming experiments (Fig. 4 and S14†). The coexisting ions above mentioned showed negligible influence on the detection of Fe^{3+} . The results confirmed that $\text{Tb}^{3+}@Zn\text{-CP}$ as a sensor can

detect Fe^{3+} even in the presence of such potential interfering ions. Similarly, $\text{Tb}^{3+}@Zn\text{-CP}$ as a sensor can detect Ru^{3+} even in the presence of such potentially interfering ions, as shown in Fig. 4 and S15.† Satisfyingly, the fluorescence response is quite quick, and it is controlled in ≤ 10 s for detecting both Ru^{3+} and Fe^{3+} (Fig. S16†).

To explore the potential selectivity of $\text{Tb}^{3+}@Zn\text{-CP}$ for various anions, potassium salts of I^- , $\text{C}_2\text{O}_4^{2-}$, CrO_4^{2-} , $\text{Cr}_2\text{O}_7^{2-}$, SO_4^{2-} , CO_3^{2-} , HCO_3^- , PO_4^{3-} and MnO_4^- were added to an aqueous of $\text{Tb}^{3+}@Zn\text{-CP}$ (10 μM) and the fluorescence of $\text{Tb}^{3+}@Zn\text{-CP}$ was observed (Fig. 5). Notably, the fluorescence intensity of $\text{Tb}^{3+}@Zn\text{-CP}$ shows a irregular quenching with addition of CrO_4^{2-} , $\text{Cr}_2\text{O}_7^{2-}$ and MnO_4^- , respectively, however other anions show a negligible influence, which indicates that $\text{Tb}^{3+}@Zn\text{-CP}$ can detect CrO_4^{2-} , $\text{Cr}_2\text{O}_7^{2-}$ and MnO_4^- selectively.

To investigate the fluorescence sensitivity ability of $\text{Tb}^{3+}@Zn\text{-CP}$ for detecting CrO_4^{2-} , $\text{Cr}_2\text{O}_7^{2-}$ and MnO_4^- , the corresponding luminescence spectra of $\text{Tb}^{3+}@Zn\text{-CP}$ (10 μM) were recorded by ion concentration titration (0.0–70 μM), as shown in Fig. S17–S19.† With the gradual addition of CrO_4^{2-} , $\text{Cr}_2\text{O}_7^{2-}$ and MnO_4^- , respectively, the fluorescence of $\text{Tb}^{3+}@Zn\text{-CP}$ were significant quenched. The influence order of three ions on luminous intensity of $\text{Tb}^{3+}@Zn\text{-CP}$ is as follows: $\text{CrO}_4^{2-} > \text{MnO}_4^- > \text{Cr}_2\text{O}_7^{2-}$, as shown in Fig. 6a and b. Quantitatively, the quenching sensitivity was quantified by the Stern–Volmer equation.⁴⁵ At low concentrations for CrO_4^{2-} (0–20 μM) and for MnO_4^- (0–30 μM), a good linearity plot was obtained with

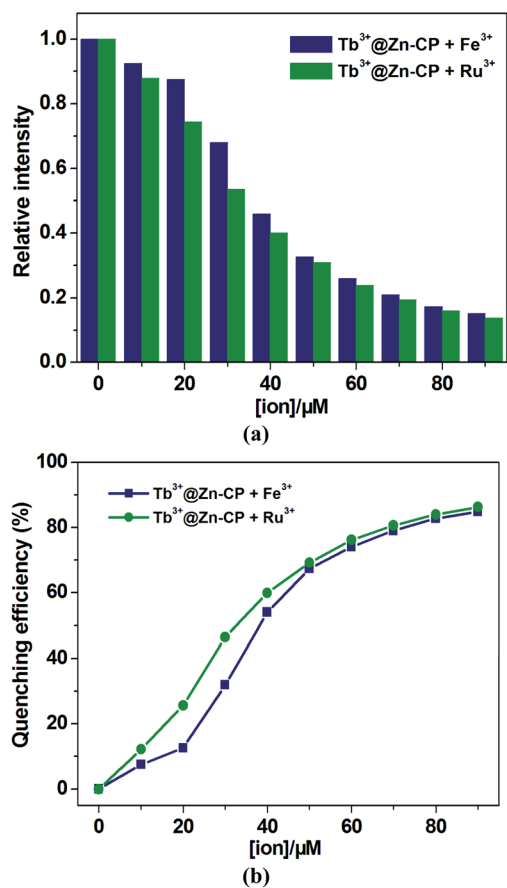


Fig. 3 (a) Relative fluorescence intensity and (b) the corresponding quenching efficiency of $\text{Tb}^{3+}@Zn\text{-CP}$ vs. different Ru^{3+} or Fe^{3+} ion concentrations. λ_{ex} : 330 nm, λ_{f} : 390 nm for $\text{Tb}^{3+}@Zn\text{-CP}$, slit width: 4 nm. [$\text{Tb}^{3+}@Zn\text{-CP}$] = 10 μM .

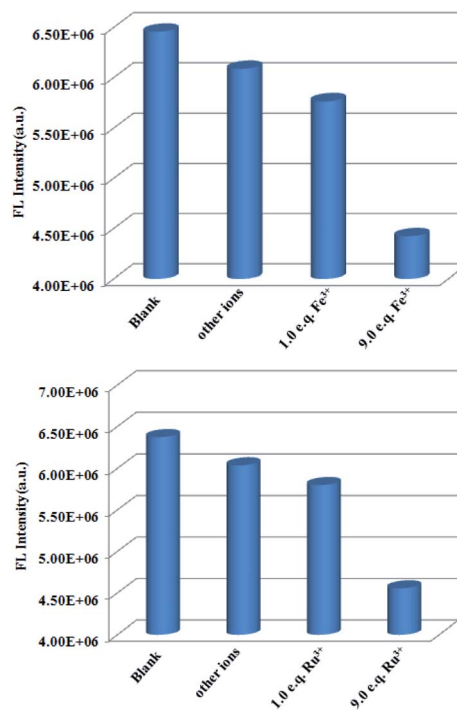


Fig. 4 Comparison of the luminescence intensity of $\text{Tb}^{3+}@Zn\text{-CP}$: after addition of mixed ions (Ag^+ , Cd^{2+} , Zn^{2+} , Pb^{2+} , Cr^{3+} , Cu^{2+} , Co^{2+} , Ni^{2+} , Mg^{2+} ; total concentration of mixed metal ions is 45 μM), and followed by addition of Fe^{3+} or Ru^{3+} ($[\text{Fe}^{3+}] = 5$ or 45 μM); ($[\text{Ru}^{3+}] = 5$ or 45 μM). λ_{ex} : 330 nm, λ_{f} : 390 nm, slit width: 4 nm.



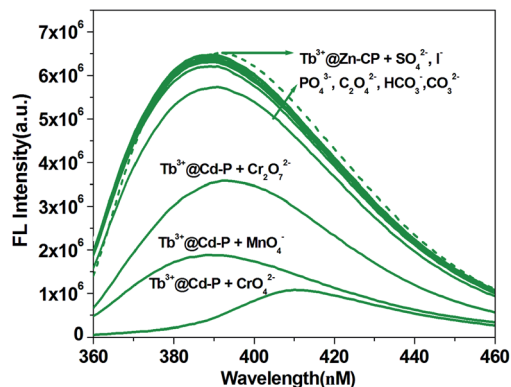


Fig. 5 Luminous intensity of Tb^{3+} @Zn-CP upon different ions (I^- , $\text{C}_2\text{O}_4^{2-}$, CrO_4^{2-} , $\text{Cr}_2\text{O}_7^{2-}$, SO_4^{2-} , CO_3^{2-} , HCO_3^- , PO_4^{3-} and MnO_4^-) in 5 mM Tris-HCl/NaCl buffer (pH 7.0) except CrO_4^{2-} (pH 8.0), $\text{Cr}_2\text{O}_7^{2-}$ (pH 6.0). [Tb^{3+} @Zn-CP] = 10 μM and [ions] = 40 μM . λ_{ex} : 330 nm, λ_{f} : 390 nm, slit width: 4 nm.

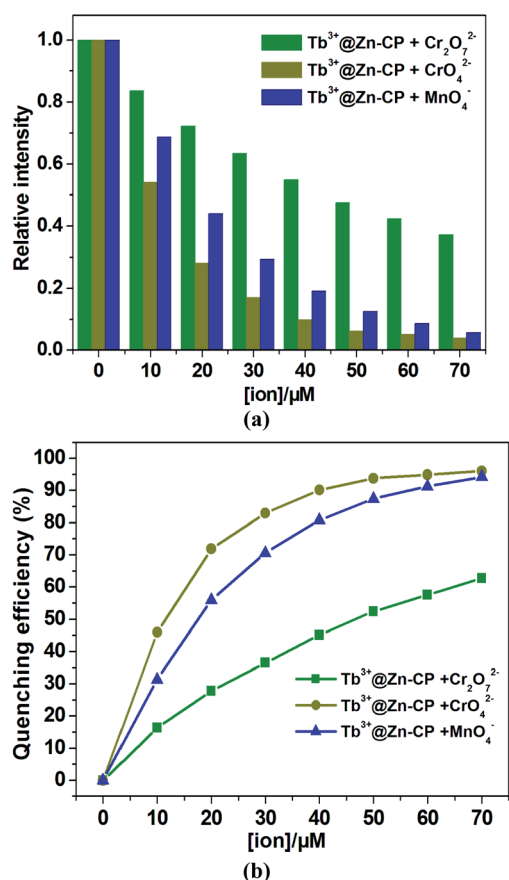


Fig. 6 (a) Relative fluorescence intensity and (b) the corresponding quenching efficiency of Tb^{3+} @Zn-CP vs. different CrO_4^{2-} (pH 8.0), $\text{Cr}_2\text{O}_7^{2-}$ (pH 6.0) and MnO_4^- (pH 7.0) ion concentrations in 5 mM Tris-HCl/NaCl buffer. λ_{ex} : 330 nm, λ_{f} : 390 nm for Tb^{3+} @Zn-CP, slit width: 4 nm. [Tb^{3+} @Zn-CP] = 10 μM .

correlation coefficient of ~ 0.99 . Also, the quenching constant (K_{sv}) were determined to be $1.18 \pm 0.16 \times 10^5 \text{ M}^{-1}$ for CrO_4^{2-} and $7.44 \pm 0.77 \times 10^4 \text{ M}^{-1}$ for MnO_4^- , respectively. However,

the Stern-Volmer plot deviated from the straight line at higher concentrations due to self-absorption or energy transfer processes.^{46,47} In addition, the LODs based on Tb^{3+} @Zn-CP were also obtained to be $0.10 \pm 0.02 \mu\text{M}$ for CrO_4^{2-} and $0.15 \pm 0.03 \mu\text{M}$ for MnO_4^- , respectively (Fig. S20a and b†). However, Fig. S20c† show that the Stern-Volmer plot for $\text{Cr}_2\text{O}_7^{2-}$ presents a good linear relationship with a correlation coefficient of 0.995. The quenching constant (K_{sv}) and the value of the detection limit ($3\sigma/k$) were evaluated to be $2.49 \pm 0.1 \times 10^4 \text{ M}^{-1}$ and $0.43 \pm 0.04 \mu\text{M}$ ($\text{S/N} = 3$), respectively, which also lies well below several MOF fluorescent sensors for detecting CrO_4^{2-} , $\text{Cr}_2\text{O}_7^{2-}$ and MnO_4^- for a specific comparison (Table S5†).

Furthermore, we measured the fluorescence response of Tb^{3+} @Zn-CP to CrO_4^{2-} , $\text{Cr}_2\text{O}_7^{2-}$ and MnO_4^- , respectively, in the presence of other anions, as shown in Fig. 7 and S21–23.† The CrO_4^{2-} , $\text{Cr}_2\text{O}_7^{2-}$ and MnO_4^- -dependent fluorescence intensity of Tb^{3+} @Zn-CP was not affected by the presence of coexisting anions such as I^- , $\text{C}_2\text{O}_4^{2-}$, SO_4^{2-} , CO_3^{2-} , HCO_3^- and PO_4^{3-} . Therefore, Tb^{3+} @Zn-CP has desirable anti-interference ability for detecting CrO_4^{2-} , $\text{Cr}_2\text{O}_7^{2-}$ and MnO_4^- . Satisfyingly, the response time is quite short, and it can control in $\sim 10 \text{ s}$ (Fig. S24†).

3.5 The underlying mechanism of luminescence quenching

The crystal integrity of Tb^{3+} @Zn-CP remained unchanged after soaking in aqueous solutions of FeCl_3 , RuCl_3 , KMnO_4 , K_2CrO_4 and $\text{K}_2\text{Cr}_2\text{O}_7$, respectively, which was confirmed by PXRD, indicating that the luminescence quenching was not caused by the collapse of the main framework structure (Fig. S5†).⁴⁹ The possible sensing mechanism of fluorescence quenching by ions were determined by further analysis.

For MnO_4^- ion detection, the result of ICP analysis show that the ratio of $\text{Zn}^{2+}/\text{Tb}^{3+}/\text{Mn}^{2+}$ is approximately 108 : 1 : 12 comparing with $\text{Zn}^{2+}/\text{Tb}^{3+}$ (80 : 1) in Tb^{3+} @Zn-CP, which ion exchange is involved in the detection of MnO_4^- by Tb^{3+} @Zn-CP (Table S3†).⁵⁰ In addition, the color of the solid sample after immersion in KMnO_4 aqueous solution was observed to have change in both ultraviolet and ordinary light, which also confirmed MnO_4^- was diffused into 2D structure of Tb^{3+} @Zn-CP (Fig. S25†). We further measured X-ray photoelectron spectroscopy (XPS) analysis on Tb^{3+} @Zn-CP after soaked in KMnO_4 , as shown in Fig. S26.† New peak at 642.5 eV appears corresponding to Mn 2p, by which the existence of MnO_4^- in the composites can be ascertained. The O 1s spectrum of Tb^{3+} @Zn-CP can be fitted into two peaks at 530.0 eV and 531.5 eV, which correspond to carboxyl group oxygen atoms and $-\text{OH}$ species, respectively (Fig. S27†). The result shows that carboxyl oxygen atoms of Zn-CP and hydroxyl oxygen atoms of H_2O participate in the formation of hydrogen bonds of MnO_4^- .²⁸ In order to examine the sensing behavior of Tb^{3+} @Zn-CP to MnO_4^- , titration experiment of Tb^{3+} @Zn-CP (10 μM) with MnO_4^- was carried out (Fig. S28†). On gradual addition of MnO_4^- (0–300 μM), the absorbance intensity of Tb^{3+} @Zn-CP solution is obviously increasing. MnO_4^- solution shows obvious absorption in the range 300–400 nm, as shown in Fig. S29.† This means that the excitation wavelength of



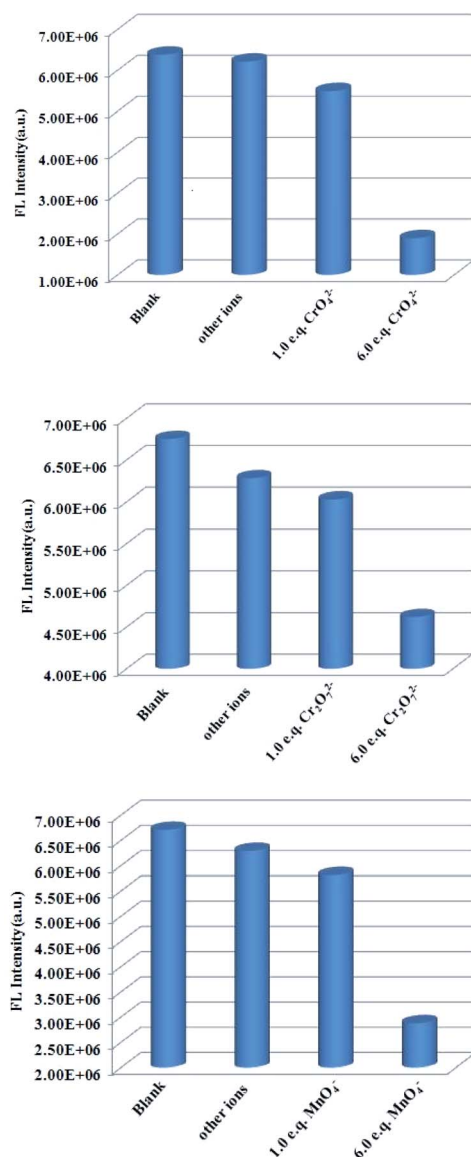


Fig. 7 Comparison of the luminescence intensity of Tb^{3+} @Zn-CP after addition of mixed ions (I^- , $\text{C}_2\text{O}_4^{2-}$, SO_4^{2-} , CO_3^{2-} , HCO_3^- and PO_4^{3-} ; total concentration of mixed ions is $30 \mu\text{M}$), and followed by addition of CrO_4^{2-} , $\text{Cr}_2\text{O}_7^{2-}$ and MnO_4^- (5 or $30 \mu\text{M}$). λ_{ex} : 330 nm, λ_{f} : 390 nm, slit width: 4 nm.

Tb^{3+} @Zn-CP is totally overlapped by the absorption spectra of MnO_4^- , which demonstrates that transfer of the excitation energy to the emissive center is effectively suppressed by MnO_4^- ions. In a word, luminescence quenching of Tb^{3+} @Zn-CP by MnO_4^- originates from three possible approaches: hydrogen bond interaction between MnO_4^- and the frameworks, ion exchange, and competitive absorption of excitation energy by MnO_4^- .^{49,50}

For CrO_4^{2-} and $\text{Cr}_2\text{O}_7^{2-}$ anion detection, we performed XPS analysis on Tb^{3+} @Zn-CP after soaked in K_2CrO_4 and $\text{K}_2\text{Cr}_2\text{O}_7$, respectively, as shown in Fig. S30 and S31.† New peak at 586.0 eV appears corresponding to Cr 2p, by which the existence of $\text{Cr}_2\text{O}_7^{2-}$, CrO_4^{2-} in the composites can be ascertained. To examine the sensing behavior of Tb^{3+} @Zn-CP to CrO_4^{2-} and

$\text{Cr}_2\text{O}_7^{2-}$, titration experiment of Tb^{3+} @Zn-CP ($10 \mu\text{M}$) with CrO_4^{2-} and $\text{Cr}_2\text{O}_7^{2-}$ were carried out. On gradual addition of $\text{Cr}_2\text{O}_7^{2-}$ (0– $300 \mu\text{M}$), the absence intensity of Tb^{3+} @Zn-CP solution is obviously increasing (Fig. S32†). With gradual addition of CrO_4^{2-} (0– $60 \mu\text{M}$), new absorption bands centered at 369 nm appeared with increasing intensity (Fig. S33†). From Fig. S29,† we can see that CrO_4^{2-} and $\text{Cr}_2\text{O}_7^{2-}$ solution show obvious absorption in the range 300–400 nm. The luminescence quenching of Tb^{3+} @Zn-CP originates from the competitive absorption of excitation energy of CrO_4^{2-} and $\text{Cr}_2\text{O}_7^{2-}$.⁵¹

For the Fe^{3+} detection process, the mechanism involving an Fe^{3+} –framework interaction, or Fe^{3+} – Zn^{2+} exchange cannot be excluded. In order to prove our hypothesis, ICP analysis of Tb^{3+} @Zn-CP after doping into Fe^{3+} was performed (Table S3†). The ratio of $\text{Zn}^{2+}/\text{Tb}^{3+}/\text{Fe}^{3+}$ is approximately 295 : 1 : 12 comparing with $\text{Zn}^{2+}/\text{Tb}^{3+}$ (80 : 1) in Tb^{3+} @Zn-CP, which ion exchange is involved in the detection of Fe^{3+} by Tb^{3+} @Zn-CP. Further, XPS analysis on Tb^{3+} @Zn-CP after soaked in FeCl_3 was performed, as shown in Fig. S34.† New peak at 711.3 eV appears corresponding to Fe 2p, by which the existence of Fe^{3+} ions in the composites can be ascertained. To examine the sensing behavior of Tb^{3+} @Zn-CP to Fe^{3+} , titration experiment of Tb^{3+} @Zn-CP ($10 \mu\text{M}$) with Fe^{3+} was carried out. On gradual addition of Fe^{3+} (0– $60 \mu\text{M}$), the absence intensity of Tb^{3+} @Zn-CP solution is obviously increasing (Fig. S35†). From Fig. S29,† we can see that Fe^{3+} also show significant absorption in the range 300–400 nm. In short, the fluorescence quenching of Tb^{3+} @Zn-CP by Fe^{3+} originates from two possible approaches: ion exchange and from the competitive absorption of excitation energy by Fe^{3+} .

For Ru^{3+} ion detection, we investigated XPS analysis on Tb^{3+} @Zn-CP after soaked in RuCl_3 , as shown in Fig. S36.† New peak at 281.8 eV appears corresponding to Ru 3d, by which the existence of Ru^{3+} in the composites can be ascertained. In addition, the color of the solid sample after immersion in RuCl_3 aqueous solution was observed to have change in ordinary light, which also confirmed Ru^{3+} was diffused into two-dimensional structure of Tb^{3+} @Zn-CP (Fig. S25†). To examine the sensing behavior of Tb^{3+} @Zn-CP to Ru^{3+} , titration experiment of Tb^{3+} @Zn-CP ($10 \mu\text{M}$) with Ru^{3+} was carried out. With gradual addition of Ru^{3+} (0– $60 \mu\text{M}$), the absence intensity of Tb^{3+} @Zn-CP solution is obviously increasing (Fig. S37†). From Fig. S29,† we can see that the solution of Ru^{3+} show obvious absorption in the range 300–400 nm. The luminescence quenching of Tb^{3+} @Zn-CP originates from the competitive absorption of excitation energy by Ru^{3+} .

Although Tb^{3+} @Zn-CP as a luminescent sensor for Ru^{3+} , Fe^{3+} , CrO_4^{2-} , $\text{Cr}_2\text{O}_7^{2-}$ and MnO_4^- , the selectivity of it is not good, because these ions might exist simultaneously in environmental samples and complicated samples such as surface water or wastewater. However, compared with Zn-CP, Tb^{3+} @Zn-CP can obviously improve the selectivity. The framework of Zn-CP contains uncoordinated nitrogen atoms and oxygen atoms possessing unshared pair electrons, which may coordinate with most metal ions or form hydrogen bonds with anions. Zn-CP is used as a parent coordination compound to encapsulate Tb^{3+} to obtain Tb^{3+} @Zn-CP. Therefore, compared with Zn-CP, there is



an obvious decrease in the adsorption capacity of Tb^{3+} @Zn-CP to metal ions and anions. In addition, compared with Zn-CP, the excitation spectrum of Tb^{3+} @Zn-CP also changed (Fig. S7†). Generally speaking, if the excitation spectrum of MOF overlaps with the ultraviolet-visible absorption spectrum of analyte to a certain extent, there is likely to be competitive energy absorption between MOF and analyte.⁵² So the competitive absorption of Ru^{3+} , Fe^{3+} , CrO_4^{2-} , $\text{Cr}_2\text{O}_7^{2-}$ and MnO_4^- is the main factor for Zn-CP fluorescence quenching.

As shown in Fig. S38 and Table S6,† the lifetime is shortened from 3.17 to 0.79 ns after Zn-CP treated with Tb^{3+} . However, the lifetimes of Tb^{3+} @Zn-CP remain in the presence and absence of Ru^{3+} , Fe^{3+} , CrO_4^{2-} , $\text{Cr}_2\text{O}_7^{2-}$ and MnO_4^- , which suggest that there are the static quenching mechanisms in selectively differentiate these ions by Tb^{3+} @Zn-CP.⁵³

4. Conclusion

We have successfully synthesized a zinc(II)-containing coordination polymer, namely $[\text{Zn}(\text{modbc})_2]_n$ (Zn-CP), using modbc as the linker. Zn-CP exhibited high stability in aqueous solution of metal salts, organic solvents and different temperatures. After encapsulation of Tb^{3+} ions in Zn-CP, the as-obtained fluorescent functionalized Tb^{3+} @Zn-CP was obtained. An investigation of sensing properties reveals that Tb^{3+} @Zn-CP as a luminescent sensor exhibits instant and selective luminescence quenching properties toward Ru^{3+} , Fe^{3+} , CrO_4^{2-} , $\text{Cr}_2\text{O}_7^{2-}$ and MnO_4^- ions in DMF/ H_2O media. It should be mentioned that the two-dimensional luminescent probes for detecting a trace amount ions (μM), well antiinterference performance, and quick response time (~ 10 s) are still few reports.

Conflicts of interest

The authors declare no competing financial interest.

Acknowledgements

This work was supported by the National Natural Science Foundation of China (No. 21571141) and Tianjin Natural Science Foundation, China (No. 15JCYBJC20300).

References

- M. Ota and C. B. Lin, *Crit. Rev. Toxicol.*, 2006, **36**, 155–163.
- E. Aakas, V. Sridis and M. Petala, *J. Environ. Sci. Health, Part A: Toxic/Hazard. Subst. Environ. Eng.*, 2013, **48**, 1390–1398.
- S. S. M. Assan, A. A. A. Shafi and A. H. K. Mohammed, *Talanta*, 2005, **67**, 696–702.
- A. Barba-Bon, A. M. Costero, S. Gil, M. Parra, J. Soto, R. Martínez-Mañez and F. Sancenón, *Chem. Commun.*, 2012, **48**, 3000–3002.
- S. K. Sahoo, D. Sharma, R. K. Bera, G. Crisponi and J. F. Callan, *Chem. Soc. Rev.*, 2012, **41**, 7195–7227.
- S. H. Hong and R. H. Grubbs, *Org. Lett.*, 2007, **9**, 1955–1957.
- R. R. Schrock, *Angew. Chem.*, 2006, **118**, 3832–3844.
- J. E. Macdonald, J. A. Kelly and J. G. C. Veinot, *Langmuir*, 2007, **23**, 9543–9545.
- M. Zheng, H. Tan, Z. Xie, L. Zhang, X. Jing and Z. Sun, *ACS Appl. Mater. Interfaces*, 2013, **5**, 1078–1083.
- B. Ding, S. X. Liu, Y. Cheng, C. Guo, X. X. Wu, J. H. Guo, Y. Y. Liu and Y. Li, *Inorg. Chem.*, 2016, **55**, 4391–4402.
- R. Lv, J. Wang, Y. Zhang, H. Li, L. Yang, S. Liao, W. Gu and X. Liu, *J. Mater. Chem. A*, 2016, **4**, 15494–15500.
- K. Akatsuka, J. W. McLaren, J. W. Lam and S. S. Berman, *J. Anal. At. Spectrom.*, 1992, **7**, 889–894.
- S. S. Nagarkar, B. Joarder, A. K. Chaudhari, S. Mukherjee and S. K. Ghosh, *Angew. Chem., Int. Ed.*, 2013, **52**, 2881–2885.
- Z. O. Tesfaldet, J. F. van Staden and R. I. Stefan, *Talanta*, 2004, **64**, 1189–1195.
- M. M. Xu, X. J. Kong, T. He, X. Q. Wu, L. H. Xie and J. R. Li, *Inorg. Chem.*, 2018, **57**, 14260–14268.
- B. Parmar, Y. Rachuri, K. K. Bisht and E. Suresh, *Inorg. Chem.*, 2017, **56**, 10939–10949.
- S. F. Tang and X. M. Hou, *Cryst. Growth Des.*, 2019, **19**, 45–48.
- B. Wang, X. L. Lv, D. Feng, L. H. Xie, J. Zhang, M. Li, Y. B. Xie, J. R. Li and H. C. Zhou, *J. Am. Chem. Soc.*, 2016, **138**, 6204–6216.
- W. Yan, C. L. Zhang, S. G. Chen, L. J. Han and H. Zheng, *ACS Appl. Mater. Interfaces*, 2017, **9**, 1629–1634.
- G. F. Ji, J. J. Liu, X. C. Gao, W. Sun, J. Z. Wang, S. L. Zhao and Z. L. Liu, *J. Mater. Chem. A*, 2017, **5**, 10200–10205.
- X. Y. Xu and B. Yan, *Sens. Actuators, B*, 2016, **222**, 347–353.
- P. C. Rao and S. Mandal, *Inorg. Chem.*, 2018, **57**, 11855–11858.
- G. Ji, J. Wang, X. Gao, J. Liu, W. Guan, H. Liu and Z. Liu, *Eur. J. Inorg. Chem.*, 2018, **19**, 1998–2003.
- Z. J. Lin, J. Lu, M. Hong and R. Cao, *Chem. Soc. Rev.*, 2014, **43**, 5867–5895.
- G. F. Ji, X. C. Gao, T. X. Zheng, W. H. Guan, H. T. Liu and Z. L. Liu, *Inorg. Chem.*, 2018, **57**, 10525–10532.
- J. N. Hao and B. Yan, *Nanoscale*, 2016, **8**, 12047–12053.
- K. M. Buschbaum, F. Beuerle and C. Feldmann, *Microporous Mesoporous Mater.*, 2015, **216**, 171–199.
- Z. Zhang, Y. He, L. Liu, X. Lu, X. Zhu, W. Wong, M. Pan and C. Su, *Chem. Commun.*, 2016, **52**, 3713–3716.
- Y. Lin, X. Zhang, W. Chen, W. Shi and P. Cheng, *Inorg. Chem.*, 2017, **56**, 11768–11778.
- R. Lv, H. Li, J. Su, X. Fu, B. Yang, W. Gu and X. Liu, *Inorg. Chem.*, 2017, **56**, 12348–12356.
- S. L. Yao, T. F. Zheng, X. M. Tian, S. J. Liu, C. Cao, Z. H. Zhu, Y. Q. Chen, J. L. Chen and H. R. Wen, *CrystEngComm*, 2018, **20**, 5822–5832.
- D. Peng, X. Xia, L. Zhao, Z. Xie, Q. Zhang, J. Jiao and G. Xu, *RSC Adv.*, 2017, **7**, 3051–3058.
- D. Basudeb, J. Rajkumar, K. B. Anup, P. R. Partha, S. Chittaranjan and H. M. Mohammad, *Inorg. Chem.*, 2019, **58**, 2686–2694.
- SHELXTL 6.10*, Bruker Analytical Instrumentation, Madison, WI, USA, 2000.
- X-Area, Version 1.44, Program Package for Single Crystal Measurements*, STOE & CIE GmbH, Darmstadt, Germany, 2008.



- 36 Y. L. Hou, H. Xu, R. R. Cheng and B. Zhao, *Chem. Commun.*, 2015, **51**, 6769–6772.
- 37 L. Li, S. Shen, R. Lin, Y. Bai and H. Liu, *Chem. Commun.*, 2017, **53**, 9986–9989.
- 38 Y. D. Wu, M. H. Lin, D. Y. Liu, M. Liu and J. Qian, *RSC Adv.*, 2019, **9**, 34949–34957.
- 39 F. Y. Yi, S. C. Wang, M. Gu, J. Q. Zheng and L. Han, *J. Mater. Chem. C*, 2018, **6**, 2010–2018.
- 40 Z. Q. Yao, G. Y. Li, J. Xu, T. L. Hu and X. H. Bu, *Chem.–Eur. J.*, 2018, **24**, 3192–3198.
- 41 C. Yu, Z. Shao and H. Hou, *Chem. Sci.*, 2017, **8**, 7611–7619.
- 42 T. K. Mondal, U. K. Ghorai and S. K. Saha, *ACS Omega*, 2018, **3**, 11439–11446.
- 43 C. Liu and B. Yan, *Photochem. Photobiol. Sci.*, 2015, **14**, 1644–1650.
- 44 L. F. Liang, L. Y. Liu, F. L. Jiang, C. P. Liu, D. Q. Yuan, Q. H. Chen, D. Wu, H. L. Jiang and M. C. Hong, *Inorg. Chem.*, 2018, **57**, 4891–4897.
- 45 Y. L. Hou, H. Xu, R. R. Cheng and B. Zhao, *Chem. Commun.*, 2015, **51**, 6769–6772.
- 46 B. Wang, X. L. Lv, D. Feng, L. H. Xie, J. Zhang, M. Li, Y. B. Xie, J. R. Li and H. C. Zhou, *J. Am. Chem. Soc.*, 2016, **138**, 6204–6216.
- 47 W. Yan, C. L. Zhang, S. G. Chen, L. J. Han and H. Zheng, *ACS Appl. Mater. Interfaces*, 2017, **9**, 1629–1634.
- 48 WHO, *Guidelines for Drinking-Water Quality*, WHO Press, Geneva, 4th edn, 2011.
- 49 P. Mahata, S. K. Mondal, D. K. Singha and P. Majee, *Dalton Trans.*, 2017, **46**, 301–328.
- 50 G. Wen, Y. Wu, W. Dong, J. Zhao, D. Li and J. Zhang, *Inorg. Chem.*, 2016, **55**, 10114–10117.
- 51 K. Fan, S. S. Bao, W. X. Nie, C. H. Liao and L. M. Zheng, *Inorg. Chem.*, 2018, **57**, 1079–1089.
- 52 D. M. Chen, N. N. Zhang, C. S. Liu and M. Du, *J. Mater. Chem. C*, 2017, **5**, 2311–2317.
- 53 B. Gole, A. K. Bar and P. S. Mukherjee, *Chem.–Eur. J.*, 2014, **20**, 2276–2291.

